High Riverine CO_2 Outgassing affected by Land Cover Types in the Yellow River Source Region

Mingyang Tian[1], Xiankun Yang[2], Lishan Ran[3], Yuanrong Su[1], Lingyu Li[1], Ruihong Yu[1], Haizhu Hu[1*], Xi Xi Lu[1,4*]

[1]Inner Mongolia key laboratory of river and lake ecology, School of ecology and environment, Inner Mongolia University, Hohhot, 010021, China

[2]School of Geographical Sciences, Guangzhou University, Guangzhou, 510006, China

[3]Department of Geography, The University of Hong Kong, Hong Kong, China

[4]Department of Geography, National University of Singapore, 117570, Singapore

✉ *Corresponding author*

Xi Xi Lu Tel.: +86-471-4991469, Fax: +86-471-4991436, e-mail: geoluxx@nus.edu.sg

Haizhu Hu Tel.: +86-471-4991469, Fax: +86-471-4991436, e-mail: huhaizhu@163.com

Abstract: Under the context of climate change, studying CO_2 emissions in alpine rivers is important because of the huge carbon storage in these terrestrial ecosystems. However, estimates of global riverine CO_2 emissions remain highly uncertain owing to absence of a comprehensive CO_2 emission measurement, especially in river source regions. In this study, riverine partial pressure of CO_2 (pCO_2) and CO_2 efflux (FCO_2) in the Yellow River source region under different landcover types, including glaciers, permafrost, wetlands, and grasslands, were investigated in April, June, August, and October 2016. Relevant chemical and environmental parameters were analyzed to explore the main controlling factors. The results showed that most of the rivers in the Yellow River source region were a net CO_2 source, with the pCO_2 ranging from 181 to 2441 μatm and the FCO_2 from -221 to 6892 g C m^{-2} yr^{-1}. Both pCO_2 and FCO_2 showed strong spatial and temporal variations. Average FCO_2 in August was higher than that in other months, with the lowest in October. In alpine climates, low temperature conditions played a crucial role in limiting biological activity and reducing CO_2 emissions. The lowest FCO_2 values (-221 g C m^{-2} yr^{-1}) were observed in the glacier and permafrost regions. By integrating seasonal changes of water surface area, total CO_2 efflux was estimated at 0.37±0.49 Tg C yr^{-1}, which is considerably higher than previous studies. Although the rivers in the Yellow River source region annually release little CO_2, there is a high carbon evasion potential. Our study suggested that the dissolved organic carbon (DOC) in permafrost rivers (5.0±2.4 mg L–1) is equivalent to that in peatland covered rivers (5.1±3.7 mg L^{-1}), and the DOC is mainly derived from old carbon stored in frozen soils. In addition, for glacial rivers with limited supply of exogenous carbon, the intensity of CO_2 emissions is still considerable. Therefore, with rising temperature due to global warming, increased CO_2 emissions in these regions should not be ignored for a better assessment of global riverine CO_2 emissions.

Key words: pCO_2, CO_2 outgassing; glaciers; permafrost; wetland; grassland; Yellow River source region

1. Introduction

Rivers connect land and oceans, acting as pipes and containers transporting carbon and other substances from terrestrial ecosystems to the oceans. Existing studies on riverine CO_2 evasion focus mainly on the spatial and temporal dynamics of partial pressure of CO_2 (pCO_2) and CO_2 efflux (FCO_2) (Cole et al.,2001; Aufdenkampe et al., 2011; Raymond et al., 2013; Abril et al., 2014). Many researchers have argued that

river water CO_2 is primarily derived from respiration of terrestrial ecosystems and decomposition of organic matter in river (Raymond et al., 2013; Hotchkiss et al., 2015; Schelker et al., 2016; Ran et al., 2017). For example, Abril et al. (2014) pointed that wetlands are the primary source of riverine CO_2 emissions in the Amazon river. However, the sources and underlying mechanisms of riverine CO_2 dynamic for many rivers remain largely unknown. Therefore, to more accurately estimate riverine CO_2 outgassing and understand its driving factors, more studies focusing on rivers in particular climates (i.e., alpine climate) and regions (e.g., headwater region or intermitted rivers) are strongly needed to gain deeper insights into global carbon balance processes.

With respect to global-scale CO_2 outgassing, available estimates are characterized by great uncertainty. For example, recent global CO_2 outgassing fluxes from rivers and streams range from 0.65 to 3.2 P g C yr^{-1} (Raymond et al., 2013; Lauerwald et al., 2015; Swakuchi et al., 2017; Drake et al., 2017), which are considerably higher than the earlier estimate by Cole et al. (2007) (i.e., 0.23 P g C yr^{-1}). A major reason for the huge range is likely the absence of a global CO_2 outgassing database which includes direct CO_2 emission measurements over different rivers and under different climate and land cover types (Raymond et al., 2013; Cole et al., 2007; Aufdenkampe et al., 2011; Drake et al., 2017). More direct field measurements are therefore strongly needed to better refine global CO_2 efflux estimates.

Yet, there have been few studies on CO_2 effluxes of rivers in extreme geographical and climatic conditions, such as alpine rivers (Wu et al., 2008; Zhang et al., 2013). Crawford et al. (2013) investigated the riverine CO_2 outgassing in the Alaska region and explored its temporal and spatial changes under different land use types. Crawford et al. (2015) further studied carbon emissions from the rivers and lakes in alpine areas around the Estes Park in the United States and found that the average pCO_2 was only 417 μatm. They concluded that high altitude and low vegetation coverage are the primary factors limiting CO_2 outgassing. Weyhenmeyer et al. (2015) concluded that production of CO_2 in lakes was usually half of the CO_2 emissions and most of the degassed CO_2 was derived from dissolved inorganic carbon (DIC). Humborg et al. (2010) surveyed rivers in central and northern Sweden and determined that the average pCO_2 and FCO_2 was 1445 μatm and 3033 g C m^{-2} yr^{-1}, respectively. Overall, compared with temperate

and tropical rivers, riverine CO_2 outgassing under alpine climate is at a relatively low level. This is largely due to the cold climate with low temperature and high altitude that hamper riverine CO_2 emissions (Peter et al., 2014).

The riverine CO_2 emissions from the Yellow River Basin have been preliminarily studied. Su et al. (2005) reported that the mainstream pCO_2 was between 1100 and 1700 μatm, which were in intermediate-low level of world rivers. The main controlling factor was its carbonate system. Zhang et al. (2008) measured the pCO_2 of 1570 μatm at Lijin Hydrological Station on the lower Yellow River during sediment regulation period (June–July), which was higher than in other periods. Zhang et al. (2009) measured the FCO_2 of the Yellow River and concluded that the Yellow River waters were a source of atmospheric CO_2 during autumn and the flux was about 0.0174 Tg C, which was similar to that of the Ottawa River but far less than that of the Amazon in autumn. Ran et al. (2015b) estimated that the annual CO_2 emissions of the whole Yellow River system at 7.9 Tg C, which is close to the basin-wide carbon deposition of 8.7 Tg C while larger than the marine import (i.e., 6 Tg C). Ran et al. (2017) further studied the Wuding River, a tributary of the middle Yellow River, and concluded that lateral carbon derived from soil respiration and chemical weathering played a central role in controlling the riverine pCO_2. In addition, radiocarbon analyses of the degassed CO_2 suggest the release of old carbon previously stored in soil horizons (Ran et al., 2018).

These studies on CO_2 emissions from the Yellow River were mainly confined to its middle and lower reaches. In contrast, to date little has been done on the upper reaches, especially the source region on the Tibetan Plateau. The Yellow River source region is located in the alpine zone with the Yellow River mainstream flowing through a variety of land cover types, including grassland, wetland, glacier, and permafrost. Affected by increasing temperature as a result of global warming, the alpine rivers in this region have become hot spots of riverine carbon cycle studies and warrant a thorough understanding of their implications for global climate change (Ulseth et al., 2018; Peter et al., 2014; Hood et al., 2015). Although Ran et al. (2015b) have estimated its pCO_2 and FCO_2 by using water chemistry data, there are no field-based direct measurements of CO_2 emissions from these alpine rivers.

To accurately determine the magnitude of riverine CO_2 outgassing and understand its underlying control mechanisms in this alpine climate region, we conducted *in situ* measurements of riverine CO_2 emissions under different land cover types, including grassland, peatland, glacier, and permafrost, in the Yellow River source region. The objectives of this study were to examine (1) the spatiotemporal patterns of CO_2 emissions under different land cover types; (2) the magnitudes of stream CO_2 emissions; and (3) the sources of riverine CO_2 in this alpine river system. Clearly, the obtained findings will lead to a greater understanding of riverine carbon export and CO_2 emissions, especially for alpine rivers, which will help refine the global estimates of riverine FCO_2.

2. Materials and methods

2.1 Site description

The Yellow River originates from the Bayanhar Mountains in Tibetan Plateau, flows through the Loess Plateau and North China Plain, and eventually empties into Bohai Sea. Generally, the drainage basin above the Tangnaihai hydrological station is called the Yellow River source region (Figure1). The study area is situated from 32°3'N 95°5'E to 36°1'N 103°3'E (Figure 1). In this region, most of the rivers flow through the Tibetan Plateau at an altitude of 3000–4000 m with meandering river channels. The study area is about 1.32×10^5 km^2, accounting for about 17.6 % of the Yellow River basin. The Yellow River source region is located in an alpine zone with a typical plateau continental climate affected by plateau monsoon (Yang et al.,1991). Its lithology is homogeneous and predominantly composed of shale and granite rocks (Chen et al., 2005). The climate is characterized by a pronounced seasonal variation with the wet season starting from June to September and the dry season from October to next May. Major land cover types of the source region include glacier, permafrost, wetland, and grassland.

Precipitation is the dominant source of runoff in the Yellow River source region. Its annual mean precipitation is 486 mm, accounting for approximately 96% of the total runoff (Liu et al., 2005). The annual evaporation varies from 800 to 1200 mm. Although the area of the source region represents only 17.6% of the whole Yellow River basin, it supplies over 33% of the basin's total water discharge (Sun et

al., 2009). In recent decades, precipitation in the source area has slightly increased owing to accelerating glacier melting (Chang et al., 2007), which has increased its relative importance of water flux for the whole Yellow River basin (Zhang et al., 2012).

2.2 Fieldwork and laboratory analyses

In this study, four fieldwork campaigns in the Yellow River source region were conducted in April, June, August, and October 2016. The riverine pCO_2 and related environmental factors, including water temperature, pH, dissolved oxygen (DO), were monitored in the field under different land cover types. In total, there are 36 sampling points (Figure 1) and they can be categorized on the basis of complexity of river network structure and land cover types (i.e., glacier, permafrost, wetland, and grassland) (Table 1). In addition, three groundwater samples in grassland covered sub-catchments were collected to determine the pCO_2 in groundwater. The temperature, pH, and DO were measured by using a Multi 3420 analyzer (WTW GmbH, Germany) with the accuracies of ±0.2 °C, ±0.004, and ±1.5%, respectively. Before measurement, the pH probe was calibrated with three pH buffers (i.e., pH4.01, pH7.00, and pH10.01, respectively).

Prior studies suggested that, when pH ranges from 7 to 10, HCO_3^- represents 96% of alkalinity and alkalinity can be used to calculate DIC (Hunt et al., 2011). Alkalinity was determined by on-site titration in this study. The collected water samples were subjected to low-pressure suction filtration through a pre-fired glass fiber filter (Whatman GF/F, GE Healthcare Life Sciences, USA) with a pore diameter of 0.7 μm. For each water sample, the alkalinity was titrated with 0.1 mol L^{-1} HCl within 12 hours after sampling. Triplicate titrations with Methyl orange as the indicator suggest that the analytical error below 3%. Beside alkalinity analysis, the remaining filtered water was transferred into 100 ml amber glass vials, poisoned with nitric acid, and preserved in refrigerator at 4 °C condition for dissolved organic carbon (DOC) measurement in laboratory. DOC was analyzed using a total organic carbon (TOC) analyzer (Elementar Analysensysteme GmbH, Germany), which has a precision better than 3%.

2.3 Determination of CO_2 emission

The CO_2 emission flux FCO_2 was measured using the floating chamber method (Ran et al., 2017) with a Li-7000 CO_2/H_2O gas analyzer (Li-Cor, Inc, USA), which has a precision better than 1%. The Li-7000 gas analyzer was calibrated with standard CO_2 gases of 500 ppm and 2000 ppm before each measurement. The rectangular floating chamber has a volume of 17.8 L and a water surface area of 0.09 m^2. The chamber walls were lowered 3 cm into water and mounted with plastic foams that had streamlined ends to limit artificial disruptions to near-surface turbulence. The chamber is covered with tin foil to reduce the influence of sun light's heating. Temperature inside chamber was measured with a waterproof thermometer. Prior to each deployment, the chamber was placed in air and the air inside the chamber was continuously circulated in a closed loop that was connected to the infrared Li-7000 gas analyzer through rubber-polymer tubes. The instrument automatically records the air CO_2 concentration and ambient atmospheric pressure. When the chamber was placed on water surface, the accumulating CO_2 concentration inside the chamber was recorded every 2 seconds, and each deployment lasted for 6–10 mins. In large rivers with relatively favorable flow conditions, the chamber was tied to a small rubber boat and freely drifted with flow to measure FCO_2. In contrast, we used the static chamber method to measure FCO_2 in small rivers or streams which may have caused an overestimation of CO_2 evasion (Lorke et al., 2015). While the chamber was freely drifting at 32 sampling sites, we used the static deployment method only at 4 sampling sites, accounting for about 10% of the all sites.

The CO_2 efflux from water was calculated using following equation (Frankignoulle et al., 1988):

$$FCO_2 = 1000 \times (dpCO_2/dt)\,(V/RTS) \quad (1)$$

where, $dpCO_2/dt$ is the slope of CO_2 change within the chamber (Pa d^{-1}; converted from μatm min^{-1}), V is the chamber volume (17.8 L), R is the gas constant, T is the chamber temperature (K), and S is the area of the chamber covering the water surface (0.09 m^2 in this study).

Surface water pCO_2 was calculated using the headspace equilibrium method (Ran et al., 2017). By using an 1100 mL conical flask, 800 mL of water were collected 10 cm below water surface and the remaining volume of 300 mL was filled with ambient air. The flask was immediately closed with a lid and

vigorously shaken for 1 min to equilibrate the gas in water and air. The equilibrated gas was then injected into the calibrated Li-7000 gas analyzer. Triplicate measurements were performed at each site and the average was calculated (analytical error below ±3%). Surface water pCO_2 was calculated based on the equations from Dickson et al. (2007):

$$pCO_2^{water,i} = pCO_2^{headspace,f} + \frac{Vh}{Vw}(pCO_2^{headspace,f} - pCO_2^{headspace,i})/K_0[1 + \frac{K_1}{[H^+]} + \frac{K_1 \cdot K_2}{[H^+]^2}]RT \quad (2)$$

where, the superscripts *i* and *f* represent the initial and final pCO_2 (μatm), *Vh* and *Vw* are the headspace volume and water volume, respectively, K_0 is the solubility of CO_2 in water calculated on the basis of solubility constants for CO_2 from *Weiss* (1974), K_1 and K_2 are the thermodynamic reaction constants (Lueker et al., 2000), $[H^+]$ represents the total concentration of hydrogen ions in final solution. *R* is the universal gas constant (8.314 J mol^{-1} K^{-1}), and *T* is the water temperature (K). Temperature in the flask after equilibration was measured to correct for temperature changes relative to that of in situ river water. The initial pCO_2 was taken as the CO_2 concentration in ambient air before the headspace equilibration measurement.

Conventionally, FCO_2 can also be estimated from the following equation.

$$FCO_2 = k \cdot K_H \cdot \Delta pCO_2 \quad (3)$$

where, *k* is the gas transfer velocity (m d^{-1}), K_H is the Henry's constant for CO_2 at a given temperature, FCO_2 is the measured riverine CO_2 efflux, and the ΔpCO_2 is the difference between the surface water and the atmosphere. Using the field-measured pCO_2 in surface water and air, *k* can be computed by rearranging Equation (3). To compare our calculated *k* value with other studies, it was standardized to a Schmidt number of 600 (k_{600}) by assigning the Schmidt number exponent to be 0.5 (Jähne et al., 1987).

We also predicted the k_{600} (m d^{-1}) through the Model 5 developed by Raymond et al. (2012).

$$K_{600} = VS \times 2841 \pm 107 + 2.02 \pm 0.209 \quad (4)$$

where, V is the stream velocity (m s^{-1}), S is the slope of rivers (unitless).

Previous studies indicate that k_{600} is affected by a number of environmental factors, such as wind speed,

slope, flow velocity, depth, and discharge (Wanninkhof et al., 1992; Zappa et al., 2007; Raymond et al., 2012). Using only flow velocity and slope of river channels would have caused overestimation for mountainous rivers due to their relatively high channel slope and thus higher flow velocity. Therefore, the extremely high k_{600} values calculated from Equation (3) were excluded from the comparison between our calculated k_{600} and the modeled k_{600}.

3.Results

3.1 Characteristics of the hydro-chemical variables

Water temperature (Tw) varied from 0.1 to 27.7 °C with an average of 11.9±5.7 °C. Average Tw in June (15.1±3.5 °C) and August (17.0±5.4 °C) was considerably higher than that in April (8.4±3.8 °C) and October (7.3±2.4 °C). Seasonal Tw difference was more significant at the wetland (14.4±6.4 °C) and grassland (12.5±5.4 °C) sites than that at the glacier (7.5±4.1 °C) and permafrost (10.0±4.0 °C) sites. Spatial variability of the air temperature was consistent with that of the water temperature at almost all the sites, although it could be as high as 33 °C. The annual average air temperature in 2016 was 16.7±6.3 °C.

Water pH ranged from 6.97 to 9.02 with an average of 7.89±0.64 (Table 1). Mean pH based on all the stream samples was 8.26±0.36, 8.55±0.45, 7.24±0.19, and 7.52±0.36 in April, June, August, and October, respectively. A slight decreasing trend can be observed with the land cover types in the order permafrost > glaciers > grassland > wetland, with the average pH value at 8.13±0.93, 7.93±0.55, 7.85±0.59, and 7.71±0.52, respectively (Table 1). Alkalinity ranged from 600 to 7600 μmol L^{-1} with an average of 2871±1381 μmol L^{-1} (Table 1). Alkalinity was higher in the cold months (3378 μmol L^{-1} in April and 2941 μmol L^{-1} in October) than in the warm months (2644 μmol L^{-1} in June and 2326 μmol L^{-1} in August).

DO values ranged from 2.7 mg L^{-1} to 12.1 mg L^{-1} and the basin-wide mean DO was 7.8±0.6 mg L^{-1} in April, 7.1±1.4 mg L^{-1} in June, 6.7±0.7 mg L^{-1} in August and 7.7±0.7 mg L^{-1} in October, respectively (Table 1). From the perspective of land cover, the highest DO values were observed at the glacier sites, with the annual average at 7.6±0.8 mg L^{-1}, followed by the permafrost sites (7.4±1.4 mg L^{-1}), the

grassland sites (7.3±0.9 mg L^{-1}), and the peatland sites (7.2±1.1 mg L^{-1}) (Table 1).

DOC ranged from 0.2 to 12.2 mg L^{-1} with an average of 4.7±2.7 mg L^{-1} (Table 1). DOC exhibited strong seasonality across the rivers. The highest DOC concentration occurred in April (5.0±1.6 mg L^{-1}), followed by August (4.9±3.6 mg L^{-1}) and June (4.7±2.9 mg L^{-1}), and the lowest was found in October (4.0±2.2 mg L^{-1}). From the perspective of land cover, the highest DOC concentrations were observed in the peatland with the annual average at 5.1±3.7 mg L^{-1}, followed by the permafrost (4.9±2.4mg L^{-1}), the grassland (4.6±2.3 mg L^{-1}), and the glaciers (3.4±1.1mg L^{-1}) (Table 1).

3.2 Spatial and temporal variations of pCO_2

The pCO_2 ranged from 181 to 2441 µatm with an average of 774±377 µatm, nearly twofold the ambient air pCO_2. To better illustrate the spatial variability pCO_2, Figures 2a, 3a, and 2c showed its changes with land cover types. The highest average pCO_2 value appeared in the peatland (937±4665-6 µatm), followed by grassland (818±394µatm), glacier (645±253 µatm), and the permafrost (600±212 µatm).

The pCO_2 value showed different temporal variation characteristics for the four land cover types (Figures 2a, 3a, and 2c). In grassland, the average river pCO_2 value in April, June, August, and October was 836±258 µatm, 609±297 µatm, 1086±551 µatm, and 734±253 µatm, respectively. In comparison, the average peatland river pCO_2 in April, June, August, and October was 875±436 µatm, 792±436µatm, 1156±630 µatm, and 926±285 µatm, respectively. The pCO_2 in these two land cover types showed the same temporal pattern with the highest pCO_2 occurring in August and the lowest in June.

Unlike in the peatland and grassland regions, the riverine pCO_2 in the glacier and permafrost regions showed relatively small variations but similar seasonal variation trends. In the glacier covered area, the average river pCO_2 value in April, June, August, and October was 635±122 µatm, 506±31 µatm, 738±449 µatm, and 632±132 µatm respectively. In the permafrost covered area, the average river pCO_2 value in April, June, August, and October was 465±216 µatm, 586±227 µatm, 591±74 µatm, and 756±231 µatm, respectively.

3.3 Spatial and temporal variations of FCO_2

CO_2 emissions exhibited spatial and seasonal variations among the 36 stream sites (Table 1, Figures 2b, 3b, and 3d). The CO_2 effluxes ranged from -221 to 1469 g C m^{-2} yr^{-1} in April, -144 to 6892 g C m^{-2} yr^{-1} in August, and -34 to 2321 g C m^{-2} yr^{-1} in October. While the highest FCO_2 was measured at the wetland sites (Site Pt 3 in August, 6892 g C m^{-2} yr^{-1}), the lowest FCO_2 was observed at permafrost sites (Site Pm 3 in April, -221 g C m^{-2} yr^{-1}) (Table 1). The averaged FCO_2 of all sites was 479±436, 261±205, 873±1220, and 714±633 g C m^{-2} yr^{-1} in April, June, August, and October, respectively. Clearly, rivers in the Yellow River source region were net carbon sources for the atmosphere, despite the great spatial and seasonal FCO_2 variations. When grouped by land cover types, the mean CO_2 efflux shows a clear decreasing trend from wetland (767±1644 g C m^{-2} yr^{-1}) through grassland (679±610 g C m^{-2} yr^{-1}) and glacier (508±588 g C m^{-2} yr^{-1}) to permafrost (302±±349 g C m^{-2} yr^{-1}). Because the intensity of CO_2 emissions depends on river pCO_2, the FCO_2 showed a similar spatial and temporal pattern to the pCO_2, although the highest and lowest pCO_2 and FCO_2 value were not found at the same sampling sites.

4. Discussion

4.1 Impact of land cover types on riverine pCO_2 and CO_2 outgassing

This study shows that the lowest FCO_2 appeared in the permafrost covered region among all land cover types, with the annual average at FCO_2 of 302±349 g C m^{-2} yr^{-1}. It is well known that a large quantity of riverine CO_2 is derived from land (Dinsmore and Billett., 2013; Hope et al., 2004). Particularly, rivers flowing through permafrost are characterized by higher organic carbon input from soils (Zeng et al., 2004), which can support higher riverine DOC export and lead to stronger CO_2 outgassing. The correlation analysis between hydro-chemical parameters and pCO_2 in the permafrost region showed that, while alkalinity, DO and DOC were not significantly correlated with pCO_2, pH exhibited a statistically significant relationship with pCO_2 (Figure 4). The negative relationship between pCO_2 and pH is likely because dissolved CO_2 itself acts as an acid in water (Stumm and Morgan., 1996). In poorly buffered systems like the study area, CO_2 can be a strong control on river water pH (Neal et al., 1998; Waldron et al., 2007). The DOC concentrations in the permafrost rivers (mean: 5.0±2.4 mg L^{-1}) were relatively

higher than that in the glacier rivers (mean: 3.6±1.1 mg L^{-1}) and the grassland rivers (4.6±2.3 mg L^{-1}) but were comparable to the peatland rivers of 5.1±3.7 mg L^{-1} in peatlands. Additionally, the average alkalinity concentration in the permafrost region is the highest among the four land cover types. However, the pCO_2 and FCO_2 values in this region were always the lowest during the four campaigns. One potential explanation is that its low temperature (i.e., annual average water temperature: 9.9 °C) because of high elevation may have constrained soil respiration and riverine organic matter degradation (Battin et al., 2008). Furthermore, although there is sufficient dissolved CO_2 in the river water, it may be difficult for CO_2 to degas from rivers in view of the low temperature (thus strong solubility) and low flow velocity (average: 0.8±0.5 m s^{-1}) (Alin et al., 2014). The lower temperature is likely the major reason for the high riverine DOC concentrations while low CO_2 outgassing rates in the permafrost region.

Because the glacier region exhibits similar temperatures and elevations to the permafrost, its pCO_2 and FCO_2 values were also relatively low, with the average only at 657±240 g C m^{-2} yr^{-1}. This is probably because all the sampling sites are located on the 1–2 order streams characterized by strong hydrologic connection with the terrestrial landscape (Sorribas et al., 2017; Smits et al., 2017), and the surrounding catchment is lack of exogenous terrestrial carbon input. The river water alkalinity of the glacier rivers showed constantly the lowest level throughout the study year (Table 1), due largely to the low coverage of carbonate rocks. For the glacier rivers, only the DOC was significantly related to pCO_2 (Figure 5d, r^2=0.56, $p < 0.001$). The glacier sampling sites are mainly located around the Aemye Ma-chhen Range (Figure 1). Wang (1998) discovered that these rivers are predominantly supplied by glacier melting that is characterized by significant seasonal variability. The sampled glacier rivers showed the lowest annual average DOC concentration among the four land cover types (3.6±1.1 mg L^{-1}). This is probably because the sub-catchments around the Aemye Ma-chhen Range do not have sufficient vegetation coverage as a result of high elevation and low temperature, limiting the terrestrial source of DOC. Poor soil, short water retention time, and low precipitation are the main reasons for the low vegetation coverage in this region (Lu et al., 2001). The rivers flowing down the snow mountain cut deep into the B horizon of soils because of strong glacial erosion and retreat. Almost all the glacial sampling sites are characterized by gravel channel, limiting the supply of terrestrial organic carbon into river carbon pools. As a result, the measured

DOC concentrations in most of the sampled glacier rivers were very low. For glacial rivers, if there is no external supply of DOC, a complete decomposition of the river water DOC can only produce 0.34 μmol L^{-1} CO_2. This suggests that the CO_2 produced by DOC degradation in the glacial river cannot maintain such a high CO_2 outgassing rate. The modern snow and ice which are important water sources in the Aemye Ma-chhen Range do not have enough DOC, DIC, or CO_2 contents (Wu et al., 2008). Instead, chemical weathering may have played a crucial role in supporting glacier riverine CO_2 (Wu et al., 2005; Wu et al., 2008). Previous studies have shown that glaciers contain large amounts of CO_2 (Meese et al., 1997) and DOC (Hood et al., 2009; Singer et al., 2012), which are important sources of CO_2 for glacial rivers. Our observations found that, with increasing distance from the glaciers, the riverine pCO_2 exhibited a decreasing trend, which is likely caused by the dilution of glacier-related pCO_2.

The FCO_2 was highest in the peatland rivers among the studied 4 land cover types. Only the pH showed a negative linear relationship with the pCO_2, while the alkalinity had a weak linear relationship with the pCO_2 (Figure 6). For peatland rivers, terrestrially-derived organic carbon has been widely recognized an important source of riverine CO_2 (Abril et al., 2014; Müller et al., 2015; Billett et al., 2015, Hu et al., 2015). There are a variety of sources for DOC in the peatland. First, the soil in the wetland ecosystem is rich in peat soil. The amount of peat stock in the Zoige Peatland is estimated to be 1.9 billion tons, accounting for about 40% of China's marsh wetland carbon storage (Wang et al., 2012). These carbon supplies to river carbon pools are an important driver for the high FCO_2 in the wetland rivers. In addition, soil pore water enriched with high concentrations of dissolved CO_2 continues to enter river waters, which can provide enough riverine CO_2 (Butman et al., 2011). Furthermore, vegetation in the peatland region can import large amounts of CO_2 into the river water through two mechanisms. On one hand, vegetation litter and root exudates release degradable organic matter into rivers. Decomposition of these organic matter serves as a carbon source for heterotrophic microorganisms. During this process, heterotrophic organisms release CO_2 into water (Abril et al., 2014). On the other hand, respiration of plant roots and soil microorganisms that are submerged in wetland soils could also release CO_2 directly into river water (Abril et al., 2014). The combined effects of these factors have resulted in rivers with high DOC and FCO_2 values in wetlands.

The average FCO_2 in the grassland rivers of 818±394 g C m^{-2} yr^{-1} is at a moderate level, lower than the wetland FCO_2 but considerably higher than that in the glacier and permafrost rivers. Correlation analyses between water chemistry parameters and riverine pCO_2 for the grassland rivers showed that both pH and DOC had weak correlations with pCO_2 (Figure 7). This also suggests that pCO_2 is partially affected by the water pH. Compared to the other three land cover types, grassland has been substantially affected by human activity (i.e., grazing). Consequently, besides the DOC derived from physical erosion, the pollutants produced by grazing are also important sources of riverine DOC. The average pCO_2 in peatland is 15% higher, but the average DOC concentration in wetland is 11% higher than that in grassland, and the alkalinity in grassland rivers is 46% higher than that in the wetland rivers. In addition, DIC is an important source of riverine CO_2 for grassland rivers. While stream DIC source are highly variable across space and time (Smits et al., 2017), most of the HCO_3^- in the Yellow River source region is derived from carbonate and silicate weathering (Wu et al., 2005; Wu et al., 2008; Wu et al., 2008), which largely reflects the contribution of groundwater inflow (Marx et al., 2017). Our groundwater samples from grassland region show an average pCO_2 of 1976 μatm, which is 2.5 times the average pCO_2 of the whole Yellow River source region. Therefore, the CO_2 excess in the grassland rivers is more likely maintained by both the terrestrial organic carbon input and the inorganic carbon from groundwater.

With respect to the k_{600}, the computed k_{600} showed statistically significant but weak correlation with the modeled results (Figure 8a) when the high k_{600} values (>70 m d^{-1}) were removed from analysis. Given the chamber's dampening effect of wind (Matthews et al., 2003), there was no any statistically significant relationship between wind and k_{600} for streams. Instead, flow velocity is a relatively good predictor of k_{600} and can approximately explain 15% of its variability (Figure 8b). Although we deployed the floating chamber very carefully, the statistical analysis could not reflect the complex interactions of various environment factors except the four land cover types through our 36 sampling sites. Additionally, it is worth noting that the Model 5 of Raymond et al. (2012) has overestimated the k_{600}, especially for mountainous rivers. This is probably because of low water temperature that has constrained CO_2 degassing although the steeper channel slope has caused stronger flow turbulence (Battin et al., 2008). A

low temperature will limit the rate of Brownian motion and reduce the CO_2 exchange with the atmosphere. Meanwhile, a low temperature will increase the solubility of dissolved CO_2, thus reducing the outgassing of CO_2.

4.2 Significance and implications for riverine carbon budgets

This study demonstrates that the annual average pCO_2 is 771±380 μatm and FCO_2 is 590±766 g C m^{-2} yr^{-1} in the Yellow River source region. In comparison, Ran et al. (2015a; 2015b) estimated a considerably lower pCO_2 value of 241±79 μatm and an areal CO_2 efflux of is -221±112 g C m^2 yr^{-1} for the Yellow River source region, indicative of a strong carbon uptake from the atmosphere. Combining the seasonal difference of water surface area between the wet season (122 days and a water surface area of 770 km^2) and the dry season (243 days and a water surface area of 560 km^2), we estimated a total CO_2 efflux from the Yellow River source region at 0.37±0.49 T g C yr^{-1}. This suggests a net carbon source for the atmosphere. Our CO_2 effluxes contrast with the earlier estimate by Ran et al. (2015b) which reported a carbon sink of -0.17±0.08 Tg C yr^{-1}.

Unlike our systematic sampling within the Yellow River source region, Ran et al. (2015b) estimated its riverine CO_2 outgassing by using only results at five sampling sites. There may have caused the huge CO_2 efflux difference. Firstly, the sampling by Ran et al. (2015b) was confined to the mainstem and major tributaries, which may have underestimated CO_2 emissions from lower-order headwater streams that usually present strong CO_2 degassing (Butman and Raymond, 2011). For example, our sampling in the Zoige peatland rivers demonstrated that the lower-order rivers exhibit substantially higher FCO_2 (767±1144 g C m^{-2} yr^{-1}) than the Yellow River mainstem (351±306 g C m^{-2} yr^{-1}). This reveals the impact of strong flow turbulence and land-river connectivity of low-order streams on sustaining the high CO_2 effluxes (Crawford et al., 2013). In addition, the importance of groundwater inflow may decline with increasing stream orders, leading to a decreasing pCO_2 and thus lower FCO_2 (Marx et al., 2017). Another potential reason is that the number of sampling sites has limited the accuracy of CO_2 emissions. This is highly possible for the Yellow River source region with the pCO_2 in groundwater (1976 μatm) 2.5 times higher than that in the river (771±380 μatm). The CO_2 originating from groundwater can be quickly

released to the atmosphere within a short distance (Hotchkiss et al., 2015). Obviously, it is considerably challenging to detect the impact of groundwater inflow without high-resolution sampling.

While the Yellow River source region occupies 17.6% of the whole Yellow River basin, it accounts for only around 4% of the basin's total CO_2 efflux (Ran et al., 2015a; 2015b). The CO_2 efflux of the Yellow River source region is also small compared with the effluxes from boreal river catchments (Teodoru et al., 2009; Butman and Raymond., 2011; Crawford et al., 2013; 2015; Kokic et al., 2015; Looman et al., 2016) or even smaller relative to the global CO_2 efflux (Aufdenkampe et al., 2011). Nevertheless, there is a huge carbon emission potential in the coming decades. Since the permafrost and wetland in the Yellow River source region are abundant in huge quantities of carbon storage. Continuously increasing temperature due to global warming will accelerate not only the mobilization of organic carbon in permafrost, but also the degradation of organic carbon by soil microorganisms. As a consequence, increasing riverine CO_2 effluxes are highly anticipated and warrant further studies to comprehensively understand their implications for global carbon cycle and climate change.

We have comprehensively evaluated the riverine carbon dynamics within the Yellow River source region by means of *in situ* measurement of CO_2 emissions under four different land cover types. However, it must be noted that there are still great uncertainties to be properly addressed in future studies. Despite the significant increase in the number of sampling sites compared with previous studies, less research on single watersheds that are spatially representative has been performed. Moreover, temporally continuous sampling involving the diel dynamics of riverine carbon export remains lacking. For example, prior studies suggest CO_2 efflux during the daytime would be completely different from that at night and floods may have a huge shift on CO_2 emissions (Geeraert et al., 2017; Smits et al., 2017).

5. Conclusions

Based on four rounds of field direct measurements of CO_2 outgassing within the Yellow River source region, the average pCO_2 in the study area was estimated at 771±380 μatm and the average FCO_2 was 590±766 g C m^{-2} yr^{-1}. The FCO_2 and pCO_2 are lower than other rivers in the world and at a relatively

low level compared to the middle and lower reaches of the Yellow River. The results showed that the rivers in the Yellow River source region were net sources of atmospheric CO_2. Both the pCO_2 and FCO_2 showed strong spatial and temporal variations. The largest riverine CO_2 efflux was found in August, followed by October and April, and the lowest was observed in June. When grouped into different land cover types, the FCO_2 in the permafrost river was the lowest among the four types of land cover. The highest FCO_2 was found in peatland rivers, followed by rivers in the grassland and glacier regions.

For the Yellow River source region with an alpine climate, the low temperature conditions have played a crucial role in limiting its biological activity and reducing CO_2 emissions. As a consequence, these procedures control both the riverine CO_2 sources and gas transfer velocity across the water-air interface. The DOC concentration acts as an important control on riverine CO_2 dynamics under all the four land cover types. In the permafrost region, the large amounts of terrestrially-derived DOC supported its high pCO_2 levels. While in the glacier region, the glacial DOC and CO_2 may have played an essential role in determining CO_2 outgassing. In the peatland and grassland regions, decomposition of plant-derived organic matter is an important source of riverine CO_2. Moreover, groundwater inflow and chemical weathering played an important role in supporting riverine CO_2 for the whole Yellow River source region.

By integrating the seasonal changes of water surface area, the riverine CO_2 efflux of the Yellow River source region was estimated at 0.37 ± 0.49 Tg C yr^{-1}, which is significantly higher than earlier estimates (e.g., -0.168 ± 0.084 Tg C yr^{-1} by Ran et al. (2015a; 2015b). To date, very few studies have focused on the dynamics of riverine carbon cycling on the Tibetan Plateau river systems. This study provides insight into the riverine CO_2 outgassing in the Yellow River source region, which will improve our current understanding of CO_2 emissions from alpine rivers in the world, in particular these located on the Tibetan Plateau.

Acknowledgements: This research was supported by the Natural Science Foundation of China (Grant No. 91547110; 51469018) and the National University of Singapore (Grant No. R-109-000-191-646; R-109-000-227-115). Special thanks go to the two anonymous reviewers for their constructive comments

which greatly improved the manuscript.

Reference

Abril, G., Martinez, J.M., Artigas, L. F., Moreira-Turcq, P., Benedetti, M. F., Vidal, L., Meziane, T., Kim, J.-H., Bernardes, M. C., and Savoye, N.: Amazon River carbon dioxide outgassing fueled by wetlands, Nature, 505, 395–398, 2014.

Alin, S. R., Maria, D. F. F. L. R., Salimon, C. I., Richey, J. E., Holtgrieve, G. W., Krusche, A. V., and Snidvongs, V.: Physical controls on carbon dioxide transfer velocity and flux in low-gradient river systems and implications for regional carbon budgets. Journal of Geophysical Research Biogeosciences, 116 (G1), 248–255, 2014.

Aufdenkampe, A. K., Mayorga, E., Raymond, P. A., Melack, J. M., Doney, S. C., Alin, S. R., Aalto, R. E., and Yoo, K.: Riverine coupling of biogeochemical cycles between land, oceans, and atmosphere. Frontiers in Ecology & the Environment, 9 (1), 53–60, 2011.

Battin, T. J., Kaplan, L. A., Findlay, S., Hopkinson, C. S., Marti, E., Packman, A. I., Newbold, J. D., and Sabater, F.: Biophysical controls on organic carbon fluxes in fluvial networks. Nature Geoscience, 1 (8), 95–100, 2008.

Billett, M. F., Garnett, M. H., and Dinsmore, K. J.: Should aquatic CO_2, evasion be included in contemporary carbon budgets for peatland ecosystems? Ecosystems, 18 (3), 471–480, 2015.

Butman, D., and Raymond, P. A.: Significant efflux of carbon dioxide from streams and rivers in the United States, Nature Geoscience, 4, 839–842, 2011.

Chang, G., Li, L., Zhu, D., Wang, Z., Xiao, J., and Li, F.: Changes and Influencing Factor s of Surface Water Resources in the Source Region of the Yellow River. Acta Geographica Sinica, (03): 312–320, 2007.

Chen, J., Wang, F., Meybeck, M., He, D., Xia, X., and Zhang, L.: Spatial and temporal analysis of water chemistry records (1958–2000) in the Huanghe (Yellow River) basin. Global Biogeochemical Cycles, 19(3), 2005.

Crawford, J. T., Striegl, R. G., Wickland, K. P., Dornblaser, M. M., and Stanley, E. H.: Emissions of carbon dioxide and methane from a headwater stream network of interior Alaska. Journal of Geophysical Research Biogeosciences, 118 (2), 482–494, 2013.

Crawford, J T., Dornblaser, M M., Stanley, E H., Clow D W., and Striegl R D.: Source limitation of carbon gas emissions in high-elevation mountain streams and lakes. Journal of Geophysical Research Biogeosciences, 120 (5): 952–964, 2015.

Cole, J. J., Cole, J. J., Caraco, N. F., and Caraco, N. F.: Carbon in catchments: connecting terrestrial carbon losses with aquatic metabolism. Marine & Freshwater Research, 52 (1), 101–110, 2001.

Cole, J. J., Prairie, Y. T., Caraco, N. F., McDowell, W. H., Tranvik, L. J., Striegl, R. G., Duarte, C. M., Kortelainen, P., Downing, J. A., Middelburg, J. J., and Melack, J.: Plumbing the global carbon cycle: Integrating inland waters into the terrestrial carbon budget, Ecosystems, 10, 171–184, 2007.

Dickson, A. G., Sabine, C. L., and Christian, J. R.: Guide to best practices for ocean CO_2 measurements. Pices Special Publication, 2007.

Dinsmore, K. J., M. F. Billett, and K. E. Dyson, Temperature and precipitation drive temporal variability in aquatic carbon and GHG concentrations and fluxes in a peatland catchment, Global Change Biol., 19 (7), 2133–2148, 2013.

Drake, T. W., Raymond, P. A., and Spencer, R. G.: Terrestrial carbon inputs to inland waters: A current synthesis of estimates and uncertainty, Limnology and Oceanography Letters, doi: 10.1002/lol2.10055, 2017.

Frankignoulle, M.: Field measurement of air-sea CO_2 exchange. Optik-International Journal for Light and Electron Optics, 33 (3), 313–322, 1988.

Geeraert, N., Omengo, F. O., Borges, A. V., Govers, G., and Bouillon, S.: Shifts in the carbon dynamics in a tropical lowland river system (Tana River, Kenya) during flooded and non-flooded conditions, Biogeochemistry, 132, 141-163, 2017.

Hood, E., Battin, T. J., Fellman, J., O'neel, S., and Spencer, R. G.: Storage and release of organic carbon from glaciers and ice sheets, Nature Geoscience, 8, 91–96, 2015.

Hood, E., Fellman J., Spencer R., Hernes P., Edwards R., Amore D., and Scoot D.: Glaciers as a source of ancient and labile organic matter to the marine environment, Nature, 462, 1044–1047, 2009.

Hope, D., S. M. Palmer, M. F. Billett, and J. J. C. Dawson, Variations in dissolved CO2 and CH4 in a first-order stream and catchment: A investigation of soil-stream linkages, Hydrological Process., 18(17), 3255–3275, 2004.

Hotchkiss, E. R., Jr, R. O. H., Sponseller, R. A., Butman, D., Klaminder, J., Laudon, H., Rosvall, M., and Karlsson.: Sources of and processes controlling CO_2 emissions change with the size of streams and rivers. Nature Geoscience, 8 (9), 2015.

Hu, J.: GHG gas emissions and spatiotemporal variation from rivers in Zoige plateau, Northwest A&F University, 2015.

Hunt, C. W., Salisbury, J. E., and Vandemark, D.: Contribution of non-carbonate anions to total alkalinity and overestimation of pCO_2 in new England and New Brunswick rivers. Biogeosciences, 8 (10), 3069–3076, 2011.

Humborg, C., C.-M. Mörth., M. Sundbom., H. Borg., T. Blenckner., R. Giesler., and V. Ittekkot.: CO_2 supersaturation along the aquatic conduit in Swedish watersheds as constrained by terrestrial respiration, aquatic respiration and weathering. Global Change Biology, 16 (7): 1966–1978, 2010.

Jähne, B., Heinz, G., and Dietrich, W.: Measurement of the diffusion coefficients of sparingly soluble gases in water. Journal of Geophysical Research Oceans, 92(C10), 10767-10776, 1987.

Kokic, J., Wallin, M. B., Chmiel, H. E., Denfeld, B. A., and Sobek, S.: Carbon dioxide evasion from headwater systems strongly contributes to the total export of carbon from a small boreal lake catchment. Journal of Geophysical Research, Biogeosciences, 120, 13–28, 2015.

Lauerwald, R., G. G. Laruelle, J. Hartmann, P. Ciais, and P. A. G. Regnier.: Spatial patterns in CO_2 evasion from the global river network, Global Biogeochem. Cycles, 29, 534–554, 2015.

Looman, A., Santos, I. R., Tait, D. R., Webb, J. R., Sullivan, C. A., and Maher, D.T.: Carbon cycling and exports over diel and flood-recovery timescales in a subtropical rainforest headwater stream. Science of the Total Environment, 550, 645–657, 2016.

Lorke, A., Bodmer, P., Noss, C., Alshboul, Z., Koschorreck, M., Somlai-Haase, C., Bastviken, D., Flury, S., McGinnis, D. F., Maeck, A., Müller, D., and Premke, K.: Technical note: drifting versus anchored flux chambers for measuring greenhouse gas emissions from running waters, Biogeosciences, 12,

7013-7024, 2015.

Lueker T, Dickson A, and Keeling C.: Ocean pCO_2 calculated from dissolved inorganic carbon, alkalinity, and equations for K1 and K2: Validation based on laboratory measurements of CO_2 in gas and seawater at equilibrium. Marine Chemistry, 70(1):105-119, 2000.

Lu, Z., Gao, H., Qiu, S., and Lin, Y.: The Remote Sensing Investigation and Research on Vegetation Coverage Characteristics and Environmental Impact in the Upper Reaches and Source Regions of the Yellow River. Shanxi Environment, 8(4):36–38, 2001.

Marx A, Dusek J, Jankovec J, Sanda, M., Vogel, T., Geldern, R.V., Hartmann, J., and Barth, J.A.C.: A review of CO_2 and associated carbon dynamics in headwater streams: A global perspective. Reviews of Geophysics, 55(2):560-585, 2017.

Matthews, C. J., St Louis, V. L., and Hesslein, R. H.: Comparison of three techniques used to measure diffusive gas exchange from sheltered aquatic surfaces. Environmental Science & Technology, 37(4), 772, 2003.

Meese, D., Gow, A., Alley, R., Zielinski, G., Grootes, P., Ram, M., Taylor, K., Mayewski, P., and Bolzan, J.: The Greenland Ice Sheet Project 2 depth-age scale: Methods and results, Journal of Geophysical Research Oceans, 102(C12):26411–26423, 1997.

Neal, C., W. A. House., H. P. Jarvie., and A. Eartherall.: The significance of dissolved carbon dioxide in major lowland rivers entering the North Sea, Science of the Total Environment, s 210–211 (1–6): 187–203, 1998.

Peter, H., Singer, G. A., Preiler, C., Chifflard, P., Steniczka, G., and Battin, T. J.: Scales and drivers of temporal pCO2 dynamics in an Alpine stream, Journal of Geophysical Research: Biogeosciences, 119, 1078–1091, 2014.

Ran, L., Lu, X X., Richey, J E., Sun, H., Han, J., Yu, Y., Liao, S., and Yi, Q.: Long-term spatial and temporal variation of CO_2 partial pressure in the Yellow River, China. Biogeosciences, 2015a, 12(4):921-932.

Ran, L., Lu, X. X., Yang, H., Li, L., Yu, R., Sun, H., and Han, J.: CO_2 outgassing from the Yellow River network and its implications for riverine carbon cycle. Journal of Geophysical Research: Biogeosciences, 2015b, 120:1334–1347.

Ran, L., Li, L., Tian, M., Yang, X., Yu, R., Zhao, J., Wang, L., Lu, X.: Riverine CO_2 emissions in the Wuding River catchment on the Loess Plateau: Environmental controls and dam impoundment impact. Journal of Geophysical Research Biogeosciences, 122 (6), 2017.

Ran, L., Tian, M., Fang, N., Wang, S., Lu, X., Yang, X., and Frankie, C.: Riverine carbon export in the arid to semiarid Wuding River carchment on the Chinese Loess Plateau. Journal of Geophysical Research Biogeosciences, 15(12), 3857-3871, 2018.

Sawakuchi, H. O., Neu. V., Ward, N.D., Barros. M., Valerio. A., Gagne-Maynard. W., Cunha. A., Less. D., Diniz. J., Brito. C., Krusche. A., and Richey. J.: Carbon dioxide emissions along the lower Amazon River, Front. Mar. Sci., 4(76), 2017.

Raymond, P.A., Zappa. C.J., Butman. D., Bott. T. L., Potter. J., Mulholland. P., Laursen. A. E., McDowell. W. H., and Newbold. D.: Scaling the gas transfer velocity and hydraulic geometry in streams and small rivers. Limnology and Oceanography: Fluids and Environments, 2(1), 2012.

Raymond, P. A., Hartmann, J., Lauerwald, R., Sobek, S., McDonald, C., Hoover, M., Butman, D., Striegl, R., Mayorga, E., and Humborg, C.: Global carbon dioxide emissions from inland waters,

Nature, 503, 355–359, 2013.
Schelker J., Singer GA., Ulseth AJ., Hengsberger S., and Battin TJ.: CO_2 evasion from a steep, high gradient stream network: importance of seasonal and diurnal variation in aquatic pCO_2 and gas transfer. Limnology & Oceanography, 61:1826–38, 2016. doi:10.1002/ lno. 10339.
Singer, G., Fasching, C., Wilhelm, L., Niggemann, J., Steier, P., Dittmar, T., Battin, T.: Biogeochemically diverse organic matter in Alpine glaciers and its downstream fate. Nature Geoscience. 5, 710–714, 2012.
Smits, A. P., Schindler, D. E., Holtgrieve, G. W., Jankowski, K. J., and French, D. W.: Watershed geomorphology interacts with precipitation to influence the magnitude and source of CO_2 emissions from Alaskan streams, Journal of Geophysical Research: Biogeosciences, 122, 1903–1921, 2017.
Sorribas, M. V., Motta Marques, D., Castro, N. M. d. R., and Fan, F. M.: Fluvial carbon export and CO_2 efflux in representative nested headwater catchments of the eastern La Plata River Basin, Hydrological Processes, 31, 995–1006, 2017.
Stumm, W., and J. J. Morgan.: Aquatic Chemistry: Chemical equilibria and Rates in Natural Waters, Cram101 Textbook Outlines to Accompany, 179 (11): A277, 1996.
Sun, W., Cheng, B., and Li, R.: Multi time Scale Correlations Between Runoff and Regional Climate Variations in the Source Region of the Yellow River. Acta Geographica Sinica, (01): 117–127, 2009.
Su, Z., Zhang, L., and Wang, X.: Influencing factors of partial pressure of CO_2 in Huanghe (Yellow River). Marine Science, 2005, (4): 41–44.
Teodoru, C. R., del Giorgio, P. A., Prairie, Y. T., and Camire, M.: Patterns in pCO_2 in boreal streams and rivers of northern Quebec, Canada. Global Biogeochemical Cycles, 23, 2009.
Ulseth, A. J., Bertuzzo, E., Singer, G. A., Schelker, J., and Battin, T. J.: Climate-induced changes in spring snowmelt impact ecosystem metabolism and carbon fluxes in an alpine stream network, Ecosystems, 21, 373–390, 2018.
Waldron, S., E. M. Scott, and C. Soulsby.: Stable isotope analysis reveals lower-order river dissolved inorganic carbon pools are highly dynamic, Environmental Science & Technology, 41(17):6156–6162, 2007. doi:10.1021/es0706089.
Wang, J.T.: Climatic Geomorphology of the Anyemaqen Mountains. Journal of Glaciology and Geocryology., 10(2):161-171,1988.
Wang, M., Liu, Z., Ma, X., and Wang, G.: Division of Organic Carbon Reserves of Peatlands in China. Wetland Science. (2): 156–163, 2012.
Wang, S., Sheng, Y., Gao, W., Li, J., Ma, S., Hu, Y.: Estimation of permafrost ice reserves in the source area of the Yellow River using landform classification, Advances in Water Science, 28 (6): 801–810, 2017.
Wanninkhof R.: Relationship between wind speed and gas exchange over the ocean.: Journal of Geophysical Research Oceans, 97(C5):7373-7382, 1992.
Weiss, R. F.: Carbon dioxide in water and seawater: the solubility of a non-ideal gas, Marine Chemistry, 2, 203–215, 1974.
Weyhenmeyer, G., Kosten S., Wallin, M., Tranvik, L., Jeppesen, E., and Roland, F.: Significant fraction of CO_2 emissions from boreal lakes derived from hydrologic inorganic carbon inputs. Nature Geoscience, 8(12):933–936, 2015.
Wu, L., Huh, Y., Qin, J., Gu, D., and Lee, S.: Chemical weathering in the Upper Huang He (Yellow

River) draining the eastern Qinghai-Tibet Plateau. Geochimica Et Cosmochimica Acta, 69(22):5279-5294, 2005.

Wu, W., Yang, J., Xu, S., and Yin, H.: Geochemistry of the headwaters of the Yangtze River, Tongtian He and Jinsha Jiang: Silicate weathering and CO_2 consumption. Applied Geochemistry, 23(12):3712-3727, 2008.

Wu, W., Xu, S., Yang, J., and Yin, H.: Silicate weathering and CO_2, consumption deduced from the seven Chinese rivers originating in the Qinghai-Tibet plateau. Chemical Geology, 249(3), 307–320, 2008.

Wu, X., Wang, N., Li, Q., Chen, L., and Jiang, X.: Ionic Compositions of Surface Snow in the Yehelong Glacier of Anyemaqen Mountains in the Headwaters of Yellow River, Journal of Glaciology and Geocryology, 30 (3): 415–420, 2008.

Yang, K.: Research on Characteristics of Precipitation and Runoff in the Upper Yellow River. Gansu Electric Power, (6): 1–14, 1991.

Zappa, C. J., Mcgillis, W. R., Raymond, P. A., Edson, J. B., Hintsa, E. J., Zemmelink, H. J., Dacey, J.W.R., and Ho. D.T.: Environmental turbulent mixing controls on air-water gas exchange in marine and aquatic systems. Geophysical Research Letters, 34(10), 373-373, 2007.

Zeng, Y., Feng, Z., Cao, G., and Xue, L.: The Soil Organic Carbon Storage and Its Spatial Distribution of Alpine Grassland in the Source Region of the Yellow River. Acta Geographica Sinica, 59(4):497-504, 2004.

Zhang, L. J., Wang, L., Cai, W. J., Liu, D. M., and Yu, Z. G.: Impact of human activities on organic carbon transport in the yellow river. Biogeosciences, 10 (4), 2513–2524, 2013.

Zhang, L., Xu, X., and Wen, Z.: Control factors of pCO_2 and CO_2 degassing fluxes from the Yellow River in autumn. Advances in Water Science, (2): 227–235, 2009.

Zhang, Y., and Wu, Y.: Analysis of Groundwater Replenishment in the Middle Reaches of Heihe River, Journal of Desert Research, 29 (2): 370–375, 2009.

Zhang, Y., Zhang, S., Zhai X., and Xia, J.: Runoff Variation in the Three Rivers Source Region and Its Response to Climate Change. Acta Geographica Sinica, (1): 71–82, 2012.

Zhang, Y.: The carbon flux and maintaining mechanism of pCO_2.Ocean University of China, 2008.

Table 1. Land cover types, altitude, stream types, pH, alkalinity, DOC, pCO_2, and FCO_2 of the 36 stream sites within the Yellow River source region, expressed in the order of April, June, August, and October in 2016.

Name	Land cover types	Apr						Jun						Aug						Oct					
		pH	Alkalinity mmol L^{-1}	DO mg L^{-1}	DOC mg L^{-1}	pCO_2 µatm	FCO_2 g C m^{-2} yr^{-1}	pH	Alkalinity mmol L^{-1}	DO mg L^{-1}	DOC mg L^{-1}	pCO_2 µatm	FCO_2 g C m^{-2} yr^{-1}	pH	Alkalinity mmol L^{-1}	DO mg L^{-1}	DOC mg L^{-1}	pCO_2 µatm	FCO_2 g C m^{-2} yr^{-1}	pH	Alkalinity mmol L^{-1}	DO mg L^{-1}	DOC mg L^{-1}	pCO_2 µatm	FCO_2 g C m^{-2} yr^{-1}
M1	grassland	8.4	4.4	7.4	4.6	662	435	8.6	2.5	6.4	2.5	513	224	7.5	-	6.6	4.7	758	794	8.6	2.9	8.1	-	643	316
M2	glacier	8.4	3.5	8.6	5.4	550	184	8.6	1.9	7.2	3.6	483	809	7.1	-	6.6	3.5	514	212	7.3	2.3	8.2	5.4	678	199
M3	grassland	8.5	4	7.5	3.9	525	451	8.7	3.1	6.8	9.5	572	28	7	-	6.4	3.8	715	497	7.8	3.1	-	1.3	535	374
GR1	grassland	7.9	1.7	8.6	3.7	886	307	8.2	2.1	6.6	1.2	538	184	7.6	2.4	7.1	3.6	1056	1603	7.3	1.8	7.4	1.4	830	589
GR2	grassland	8.5	4.8	6.8	5.9	571	583	8.6	-	7.3	5.3	488	49	7.8	-	6.5	-	1095	1607	7.3	3.7	7.6	3.1	822	724
GR3	grassland	8.2	2.8	7.1	10.0	686	297	8.2	2.1	8.6	5.1	1490	98	7.1	2.8	5.9	8.2	611	120	8	1.6	5.9	4.7	719	202
GR4	grassland	8.6	4.2	6.7	3.6	614	175	8.7	3	6.7	5.4	479	71	7	2.7	6.0	6.9	552	524	7.3	3.9	8.0	6.6	510	1361
GR5	grassland	8.4	4.4	7.5	-	969	1426	8.5	2.9	6.8	3.8	545	282	7.1	2.9	5.8	2.7	1197	1956	7.7	3.9	8.1	1.7	-	-
GR6	grassland	8.4	5.6	8.4	4.7	762	500	8.5	3.7	7.6	9.6	628	727	7.2	3.9	6.3	8.4	1863	1619	7.3	5.1	8.4	4.2	1084	2174
GR7	grassland	8.2	6.3	7.0	2.5	1393	889	8.2	3.2	6.5	3.0	608	438	7	3.5	6.9	2.8	2196	1478	7.2	5.5	8.2	1.7	1216	2321
GR8	grassland	8.2	2.6	8.3	7.4	720	199	8.8	1.9	9.0	7.8	478	331	7.2	2.8	7.3	2.6	1416	923	7.2	2.8	7.4	5.3	593	457
GR9	grassland	8.1	2.3	8.7	4.8	921	138	8.5	1.6	7.0	6.8	493	641	7.1	1.7	6.4	2.0	585	524	7.2	1.9	7.6	6.7	515	533
GR10	grassland	8	3.4	8.0	3.5	1124	1036	8.6	2.2	6.7	2.3	469	454	7.1	1.9	6.2	2.7	676	175	7.3	2.4	7.9	2.4	496	236
GR11	grassland	8.5	4.6	7.9	4.9	547	230	8.7	3	6.9	-	482	178	7.2	-	6.2	6.6	700	402	7.8	4.1	7.7	-	557	441
Pt1	peatland	8.6	4.8	7.3	6.3	562	448	8.6	3.4	6.0	4.5	522	107	7	3.6	6.5	2.5	1970	1358	-	3.5	7.1	5	876	1193
Pt2	peatland	8.2	5	8.5	6.3	1362	1128	8.2	3.3	8.3	3.0	598	61	7.1	1.8	6.5	6.1	1461	328	7.3	2.6	7.6	3.8	862	1251
Pt3	peatland	7.4	1	7.6	-	1809	831	7.9	-	6.6	1.4	1139	527	7.4	1.1	6.4	2.4	862	6892	8	1.2	7.4	6.8	1370	1818
Pt4	peatland	8.4	5.9	8.4	5.3	511	383	8.6	3.5	8.2	2.6	509	251	7.3	3.5	7.5	3.8	882	129	7.3	4.2	8.8	0.2	517	175
Pt5	peatland	7.7	1	7.0	5.1	576	282	8.6	1.5	7.1	7.6	660	273	7.1	1.8	6.3	4.2	523	92	7.2	1.7	7.8	4.4	856	650

Pt6	peatland	7.5	0.6	8.0	4.3	1177	1015	7.9	1.2	6.3	9.4	652	221	7.1	0.8	5.9	3.1	632	546	7.6	0.9	7.0	4.6	1206	1515
Pt7	peatland	7.6	0.7	8.2	-	612	1469	8.2	1.5	7.0	-	490	267	7.2	1.3	5.5	3.5	755	1778	7.5	1	8.0	3.2	685	123
Pt8	peatland	7.6	1.1	7.8	6.3	712	454	8.2	1.3	6.4	-	567	172	7.2	1.2	6.2	2.1	2441	1226	7.9	1.2	7.6	3.9	732	2030
Pt9	peatland	8.6	4.8	8.1	6.6	562	34	8.1	-	-	12.2	891	307	7.1	2.1	7.5	21.7	1268	61	7.3	-	7.1	5.1	1338	346
Pt10	peatland	7.8	1	7.1	5.1	865	126	8.5	1.6	-	3.0	1891	89	7.1	-	7.5	3.4	761	233	-	1.1	7.2	-	815	478
GL1	glacier	8.4	3.9	7.2	4.4	656	1190	-	-	-	-		-	7.6	1.2	8.3	2.1	273	-144	7.2	2.9	9.8	4.8	806	454
GL2	glacier	8.2	1.8	8.7	4.7	859	1318	8.6	-	7.5	2.0	484	83	7.5	-	6.6	-	628	392	7.5	-	7.7	-	711	399
GL3	glacier	8.5	3.1	8.2	4.7	606	156	8.7	2.3	6.8	2.8	492	52	7.3	1.9	6.4	4.5	692	583	7.8	2.5	8.0	3.9	523	230
GL4	glacier	8.4	3.1	8.1	2.7	514	205	-	-	-	-	-	-	7.5	2.1	6.6	4.5	716	328	7.8	3.1	8.4	4.6	672	328
GL5	glacier	8.5	3.1	7.5	4.1	630	46	-	-	-	-	-	-	7.3	2.2	6.9	2.9	525	1119	7.3	-	7.8		441	175
GL6	glacier	8.5	4	7.2	3.9	542	405	8.6	-	6.9	1.2	542	264	7.3	2.8	-	2.2	1592	2459	-	2.3	7.9	4	640	632
Pm1	permafrost	8.8	3.2	-	3.4	236	-141	10.6	7.4	12.1	-	-	-	7.3	2.9	6.7	6.5	560	18	7.2	-	8.5	-	936	101
Pm2	permafrost	8.6	4.1	-	5.5	511	426	8.7	-	6.2	5.1	483	138	7.2	3	5.7	8.2	538	270	8.1	7.6	6.4	-	927	933
Pm3	permafrost	8.8	5.2	-	6.3	681	267	9	-	7.2	5.0	447	44	7.2	-	6.9	7.1	554	149	-	4.1	7.2	3.8	365	-34
Pm4	permafrost	8.3	3.2	8.0	2.8	495	254	8.5	-	6.7	1.5	508	126	7.2	-	6.4	2.5	628	316	-	2.2	8.4	1.1	583	227
Pm5	permafrost	8.3	4.3	7.7	4.6	688	322	8.7	3.4	6.9	4.8	502	374	7.2	3.1	7.4	7.1	726	757	7.2	4.4	8.0	10.6	859	806
Pm6	permafrost	8.3	2.1	7.3	7.4	181	-221	8.5	2.5	6.2	4.6	989	478	7.3	1.8	9.2	6.5	540	98	-	2.6	7.0	1.4	866	1233

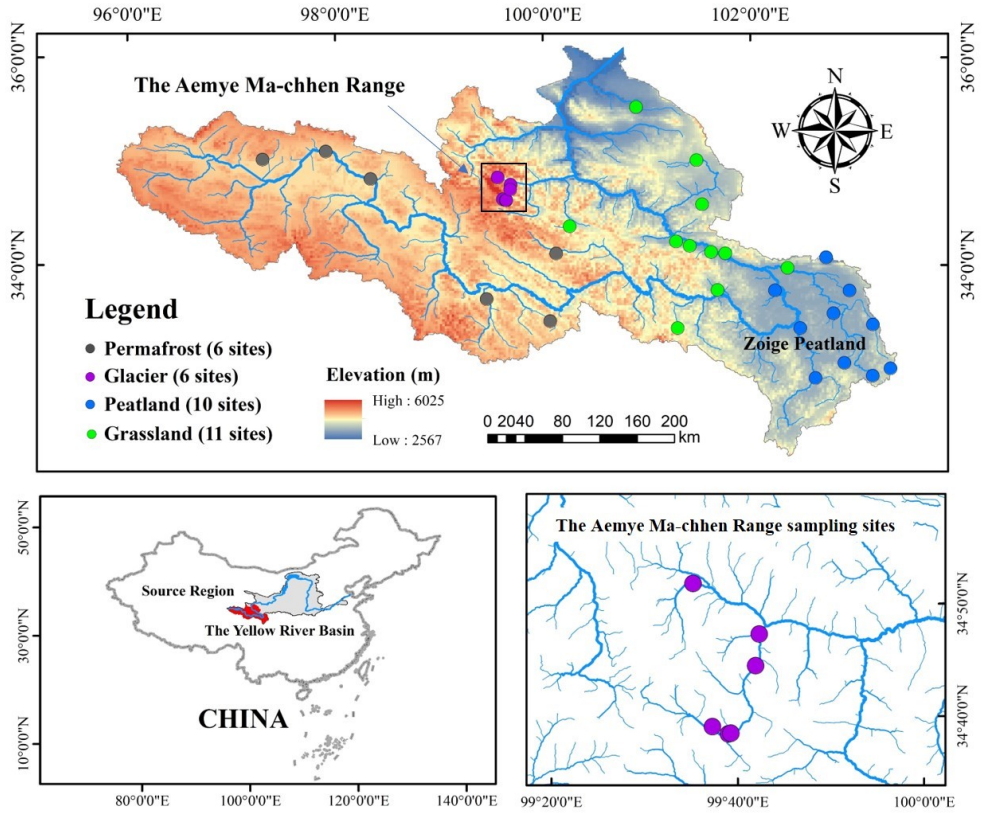

Figure 1. Sampling sites of the Yellow River source region

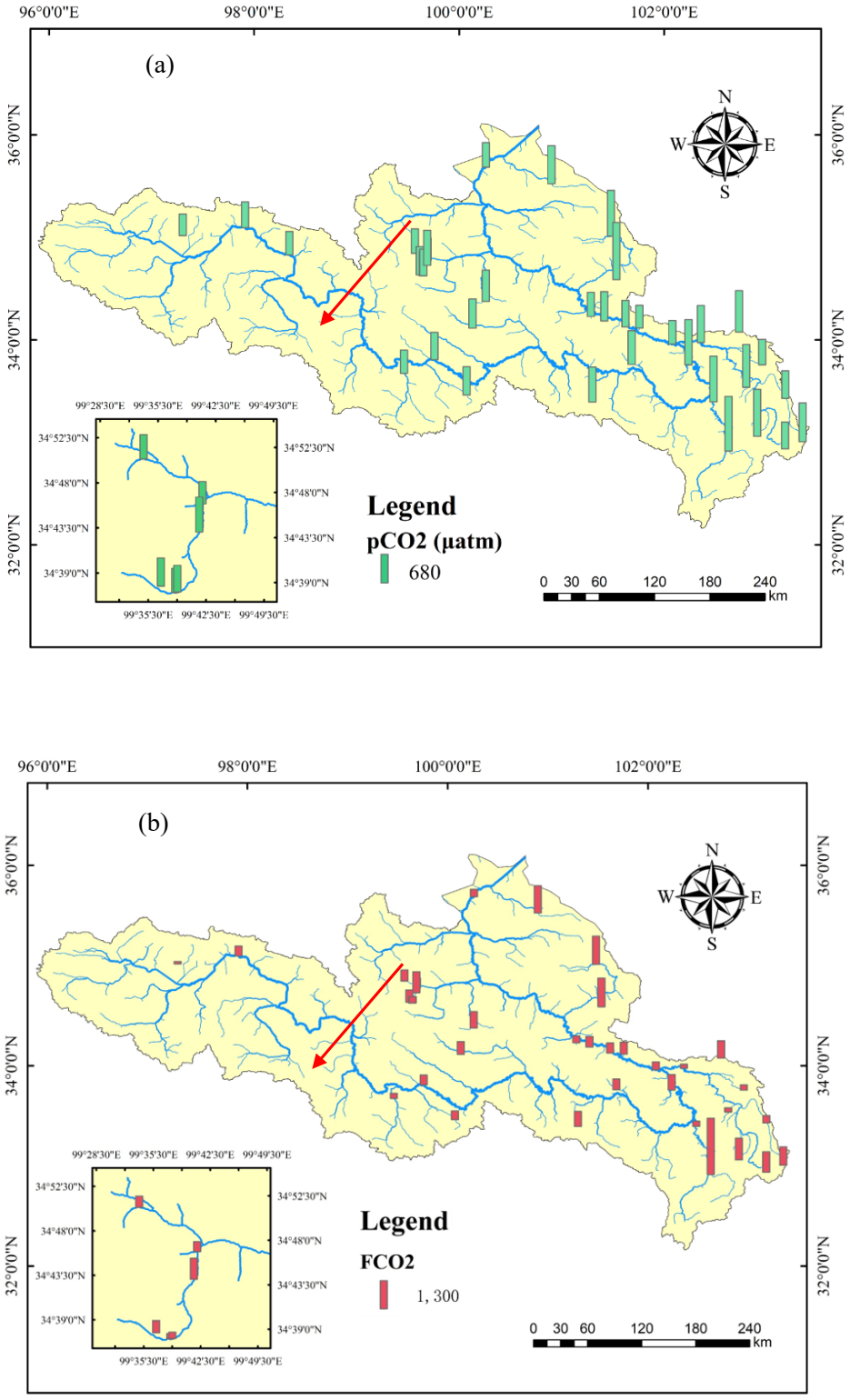

Figure 2. Spatial and temporal variations of annual average pCO_2 (a) and FCO_2 (b) within the Yellow River source region in 2016.

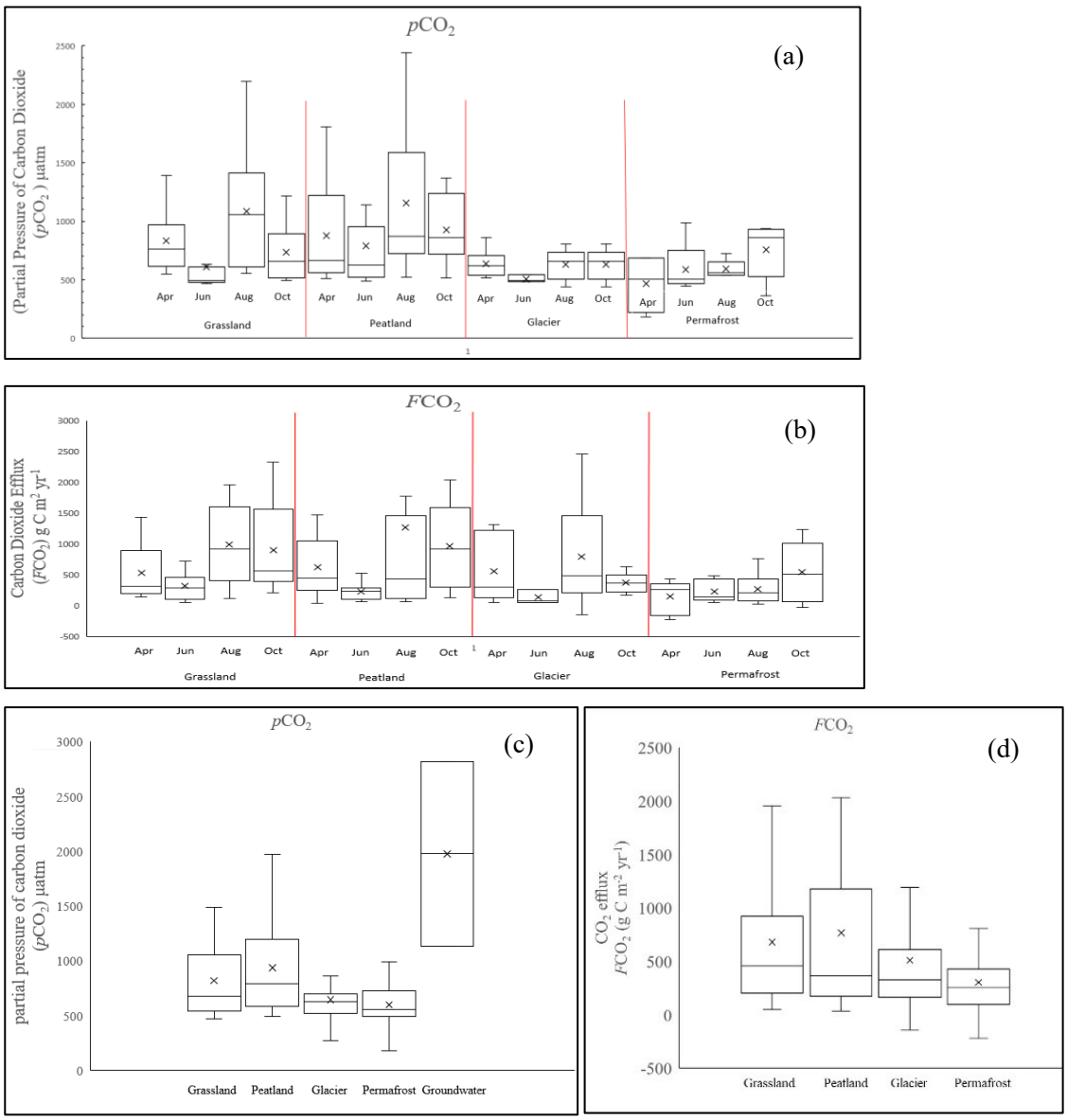

Figure 3. The box plots of pCO_2 and FCO_2 under four different land cover types within the Yellow River source region, expressed in the order of April, June, August, and October of 2016 (a and b). The pCO_2 data expressed in the order of grassland, peatland, glacier, permafrost, and groundwater (c), The FCO_2 expressed in the order of grassland, peatland, glacier, and groundwater (d).

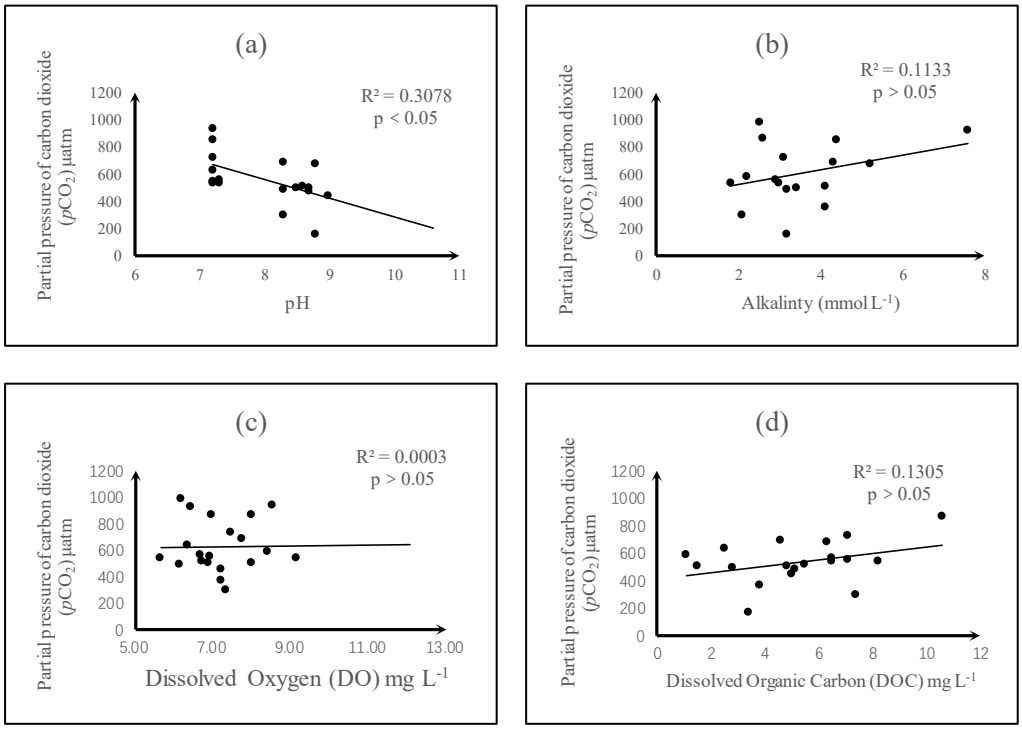

Figure 4. The linear relationship of hydro-chemical parameters and pCO_2 in permafrost covered region. (a) pH, (b) alkalinity, (c) dissolved oxygen, and (d) dissolved organic carbon.

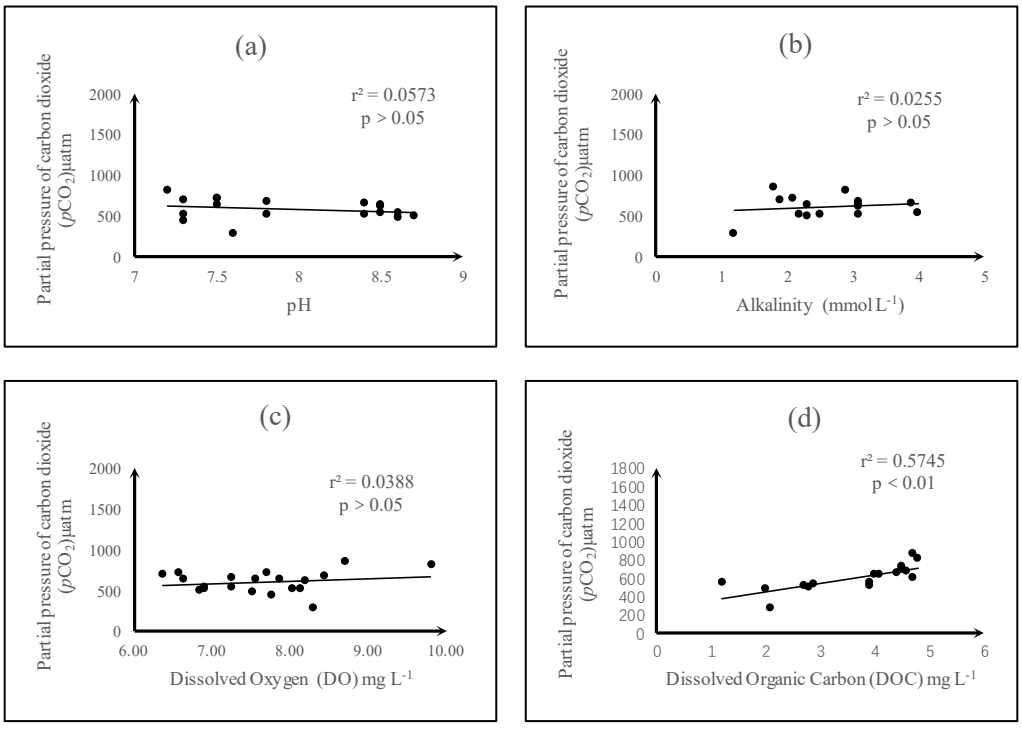

Figure 5. The linear relationship of hydro-chemical parameters and pCO_2 in glacier covered region. (a) pH, (b) alkalinity, (c) dissolved oxygen, and (d) dissolved organic carbon.

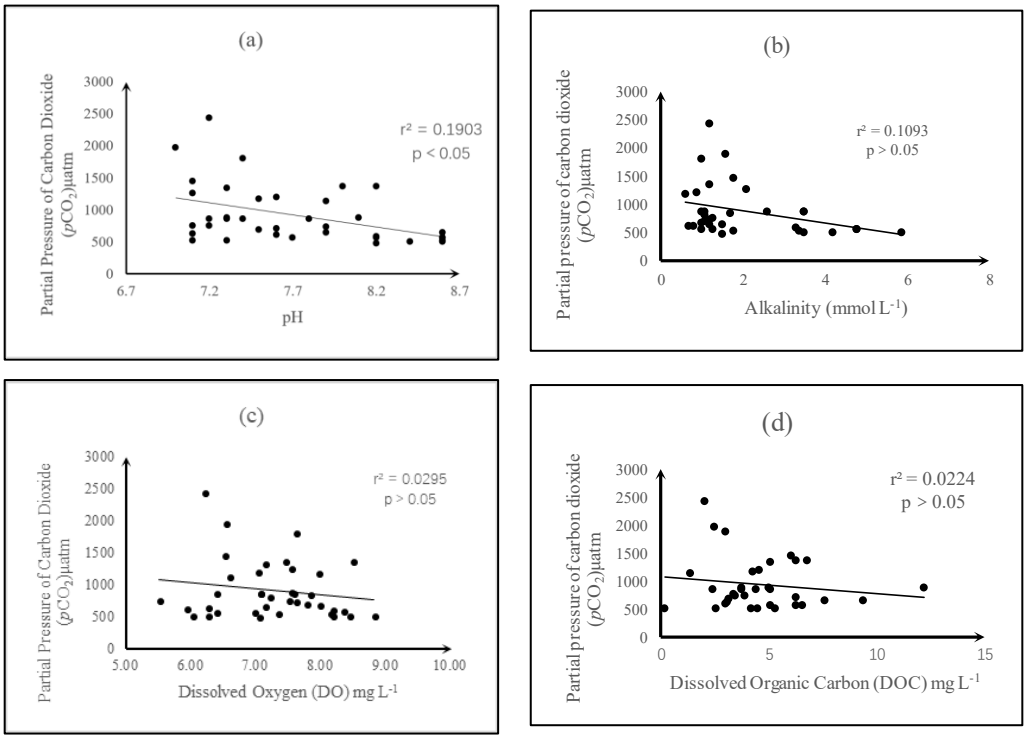

Figure 6. The linear relationship of hydro-chemical parameters and pCO_2 in peatland covered region. (a) pH, (b) alkalinity, (c) dissolved oxygen, and (d) dissolved organic carbon.

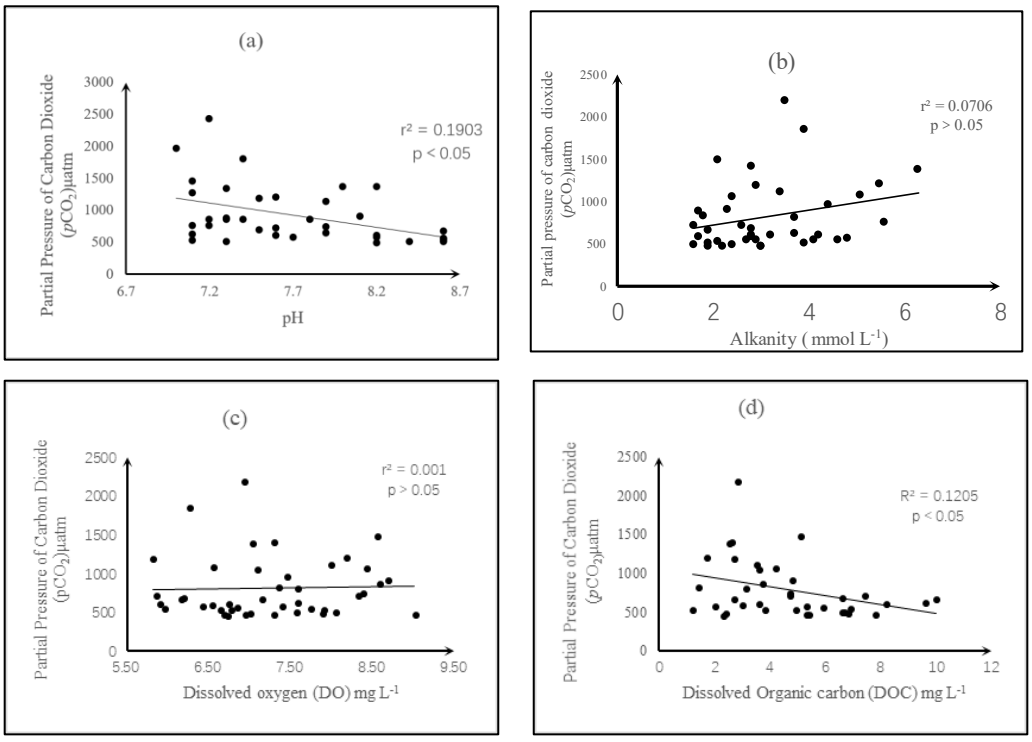

Figure 7. The linear relationship of hydro-chemical parameters and pCO_2 in grassland covered region. (a) pH, (b) alkalinity, (c) dissolved oxygen, and (d) dissolved organic carbon.

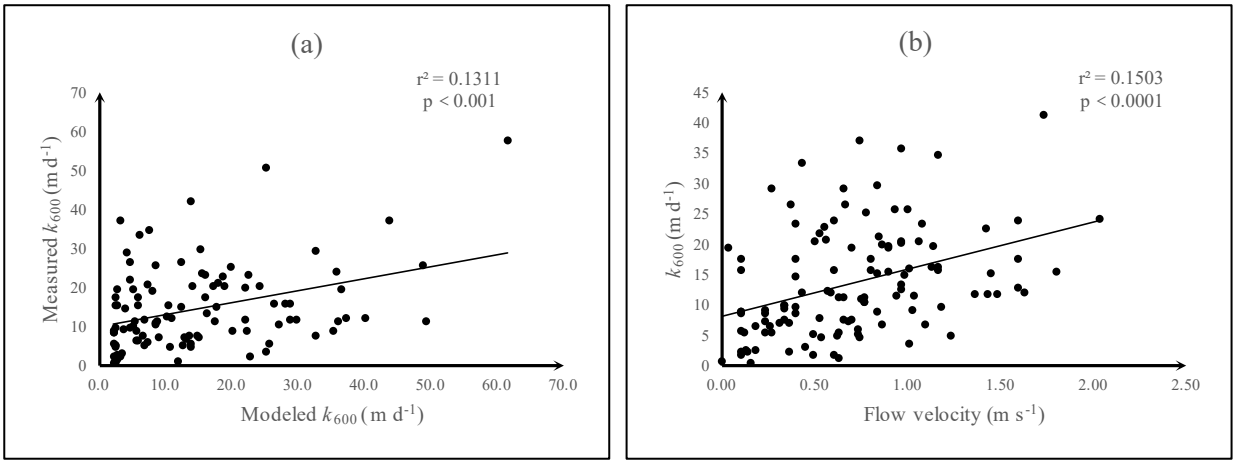

Figure 8. (a) The relationship between actual measurements (based on *in situ* pCO_2 and FCO_2) and predicted k_{600} using the Model 5 of Raymond et al. (2012) for streams; (b) Correlation between standardized (based on *in situ* pCO_2 and FCO_2) gas transfer velocity (k_{600}) and flow velocity over the 4 campaigns of field sampling.